Long-distance correlations in molecular orientations of liquid water and shape-dependent hydrophobic force

J. Maruthi Pradeep Kanth,* Satyavani Vemparala,† and Ramesh Anishetty‡
The Institute of Mathematical Sciences, C.I.T.Campus, Tharamani, Chennai 600113, India
(Received 2 September 2009; revised manuscript received 20 October 2009; published 9 February 2010)

Liquid water, at ambient conditions, has short-range density correlations which are well known in literature. Surprisingly, large scale molecular-dynamics simulations reveal an unusually long-distance correlation in "longitudinal" part of dipole-dipole orientational correlations. It is nonvanishing even at 75 Å and falls off exponentially with a correlation length of about 24 Å beyond solvation region. Numerical evidence suggests that the long-range nature of dipole-dipole correlation is due to underlying fluctuating network of hydrogen bonds in the liquid phase. This correlation is shown to give a shape dependant attraction between two hydrophobic surfaces at large distances of separation and the range of this attractive force is in agreement with experiments. In addition it is seen that quadrupolar fluctuations vanish within the first solvation peak (3 Å).

DOI: 10.1103/PhysRevE.81.021201 PACS number(s): 61.20.Ja, 61.25.Em, 82.30.Rs, 87.15.ad

Water molecule with its hydrogens and lone pairs in tetrahedral arrangement makes hydrogen bonds with its neighboring molecules. In the liquid phase the hydrogen-bond pattern undergoes rapid fluctuations at picosecond time scales [1–3], thus resulting in large orientational entropy. It is well known that this special property bestows liquid water with some unique properties, in particular the hydrophobic force of attraction between nonpolar solutes [4]. Clever experiments have been performed to measure quantitatively the distance properties of the hydrophobic force between macroscopic surfaces [5,6]. Understanding these distance properties is necessary initial step to develop a proper theory for bulk liquid water. We make an attempt toward the same in this work using molecular-dynamics (MD) simulations and general principles of statistical mechanics.

A water molecule can be modeled as a set of five points corresponding to neutral oxygen O, two positively polarized hydrogens H_1, H_2 and two negatively polarized lone-pair sites L_1, L_2 placed at tetrahedral angles about the oxygen atom. The angles between vectors $\vec{H}_{1,2}$ and $\vec{L}_{1,2}$ and length of each of them can fluctuate (vectors are defined with respect to the position of oxygen O). Such a molecule's orientations can be conveniently described with a choice of vectors defined as:

$$\vec{e}_{1(2)}(\mathbf{r}) = \frac{\vec{H}_1 + \vec{H}_2}{|\vec{H}_1 + \vec{H}_2|} - (+)\frac{\vec{L}_1 + \vec{L}_2}{|\vec{L}_1 + \vec{L}_2|} \tag{1}$$

where $\mathbf{r}$ is the position of oxygen atom in the bulk. The choice of $\vec{e}_1(\mathbf{r})$ and $\vec{e}_2(\mathbf{r})$ is such that they do not depend upon bond lengths of the molecule; they are symmetric with respect to hydrogens and lone pairs of the molecule. $\hat{e}_1(\mathbf{r})$, $\hat{e}_2(\mathbf{r})$ and $\hat{e}_3 \equiv \hat{e}_1 \times \hat{e}_2$ are the corresponding orthonormal vectors. Here $\hat{e}_1(\mathbf{r})$ is dominantly along the direction of dipole field and $\hat{e}_2(\mathbf{r})$ exists only if the water molecule differs from its mean (near-tetrahedral) geometry i.e., it is proportional to the quadrupole moment of the molecule.

The $\hat{e}$ vectors [Eq. (1)] form a complete triad with which orientation of any vector ($\vec{H}_{1,2}$ or $\vec{L}_{1,2}$) can be specified. Consequently dynamics of water can be understood to be an interacting system of the $\hat{e}$-vector fields. In particular MD simulation of water molecules implicitly gives us the dynamics of these fields. There upon various statistical correlations involving $\hat{e}_1(\mathbf{r})$, $\hat{e}_2(\mathbf{r})$ and $\rho(\mathbf{r}) \equiv (\hat{e}_1(\mathbf{r}))^2 = (\hat{e}_2(\mathbf{r}))^2$ in the liquid phase of water can be formulated as follows:

$$\langle \rho(\mathbf{r}_1)\rho(\mathbf{r}_2)\rangle = g(r) \tag{2a}$$

$$\langle \rho(\mathbf{r}_1)\hat{e}_a(\mathbf{r}_2)\rangle = \frac{\mathbf{r}}{r} d_a(r) \tag{2b}$$

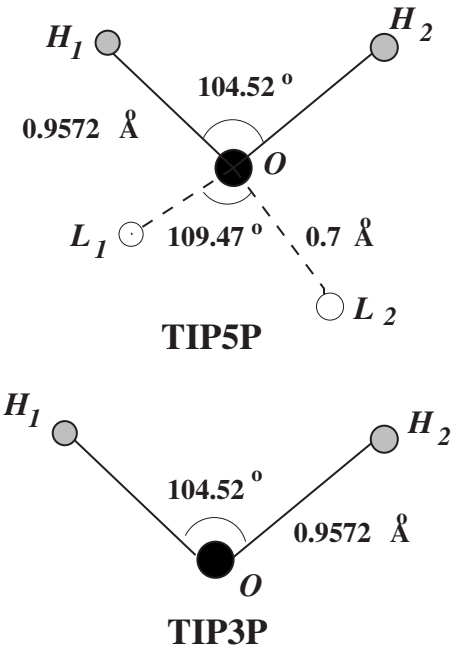

FIG. 1. Geometry of a water molecule used in TIP5P, TIP3P models.

*jmpkanth@imsc.res.in
†vani@imsc.res.in
‡ramesha@imsc.res.in

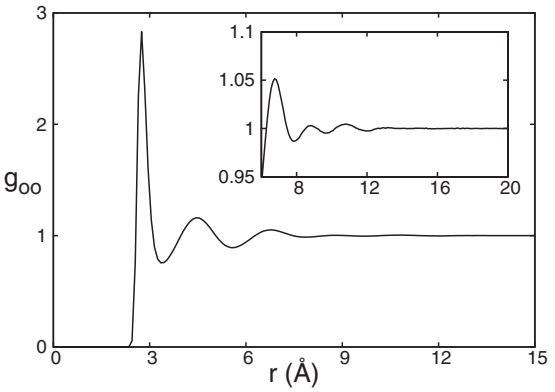

FIG. 2. TIP5P: $g(r)$. Oxygen-oxygen radial distribution function. (*inset*) additional troughs in end-solvation region.

$$\langle e_a^i(\mathbf{r}_1)e_b^j(\mathbf{r}_2)\rangle = \frac{1}{2}\left(\delta^{ij} - \frac{r^i r^j}{r^2}\right)t_{ab}(r) - \frac{1}{2}\left(\delta^{ij} - 3\frac{r^i r^j}{r^2}\right)l_{ab}(r) \tag{2c}$$

where $\mathbf{r}=(\mathbf{r}_1-\mathbf{r}_2)$, $r=|\mathbf{r}|$; subscripts $a,b=1,2,3$ (denote either of $\hat{e}_1,\hat{e}_2,\hat{e}_3$) and vector indices $i,j=1,2,3$ (denote directions in three-dimensional space).

The translational and rotational symmetry of the system enables decomposing the tensorial properties of these correlations explicitly and thus analyze the data in terms of simple scalar functions like $g(r)$, $d_a(r)$, $t_{ab}(r)$, $l_{ab}(r)$. The function $g(r)$ is the radial distribution function and it portrays distance-dependent density correlations only (here, of oxygen). The remaining functions capture the correlations among other degrees of freedom of the vector fields.

TIP5P model [7,8] possesses all orientational degrees of freedom of a water molecule and has improved accuracy in predicting the structural properties of water at ambient conditions (Fig. 1). The simulations of TIP5P water system are performed with GROMACS (version 3.3.1) package [9] with an integration time step of 2 fs. The fast-moving bonds O-H are constrained using LINCS algorithm. A large system consisting of 110592 molecules in a 150 Å box is equilibrated for 2 ns in constant pressure (isotropic and 1 atm) and temperature (300 K) *NPT* ensemble followed by a production

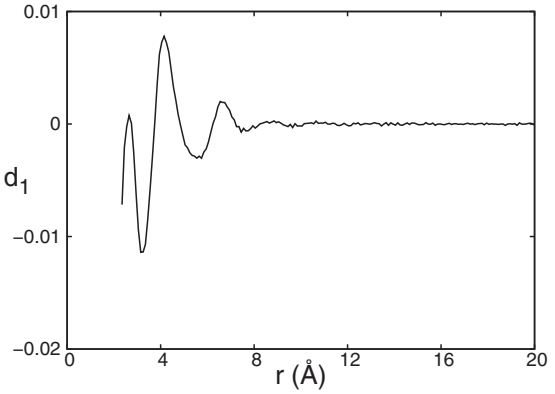

FIG. 3. TIP5P: $d_1(r)$. Oxygen-dipole correlation function vanishes beyond 14 Å

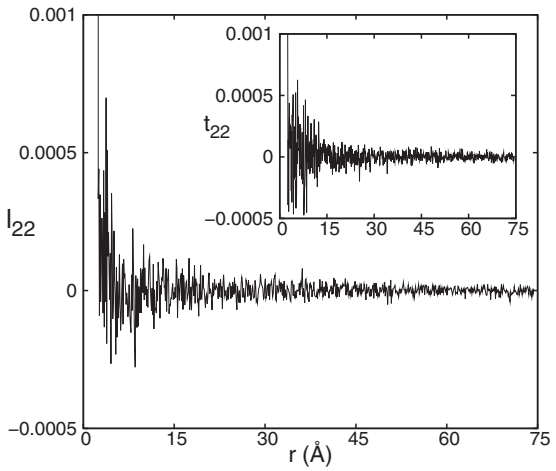

FIG. 4. TIP5P: l_{22}, (*inset*) t_{22}. Longitudinal and transverse parts of correlation $\langle \hat{e}_2\hat{e}_2\rangle$, vanishing upto statistical errors after the first solvation peak

run of 2 ns in a constant volume *NVT* ensemble. The configurations are saved every 100 ps for analysis. A cutoff distance of 12 Å and a pair-list distance of 15 Å are used to compute all nonbonded interactions and periodic boundary conditions are imposed. Full electrostatic interactions are computed with particle mesh Ewald (PME) method with a tolerance of 10^{-6} and updated every two time steps [10,11].

Density correlation $g(r)$ of TIP5P displays all the well-known solvation peaks; in addition, due to large system size and hence better statistics, few more prominent troughs are observed at about $r=8.0$ Å and $r=10.0$ Å (Fig. 2). The dipole-oxygen correlation $d_1(r)=\langle \hat{e}_1(\mathbf{r}_1)\cdot\hat{\mathbf{r}}\rho(\mathbf{r}_2)\rangle$ also exhibits its solvation structure and vanishes beyond 14 Å (Fig. 3). It is also found that correlations involving $\hat{e}_2$, $\hat{e}_3$ all vanish upto statistical errors beyond the first solvation peak itself (Figs. 4–8). Therefore $\hat{e}_2$, the quadrupole moment of the water molecule, fluctuates locally and randomly without any nonlocal correlations. While $\hat{e}_3$ being a pseudovector has vanishing correlations with $\hat{e}_1$ and $\hat{e}_2$ demonstrating that there is no parity violation in the system.

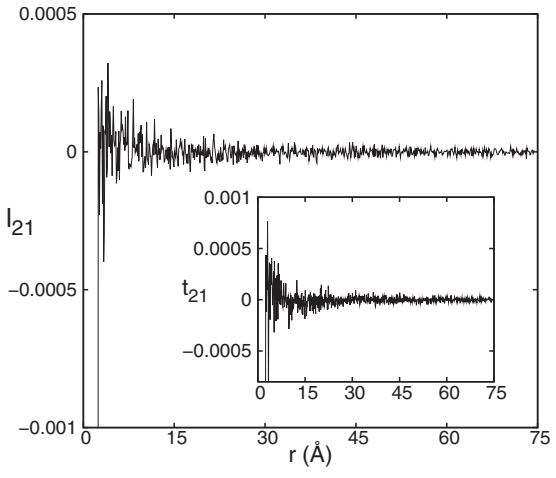

FIG. 5. TIP5P: l_{21}, (*inset*) t_{21}. Longitudinal and transverse parts of correlation $\langle \hat{e}_2\hat{e}_1\rangle$, vanishing upto statistical errors after the first solvation peak

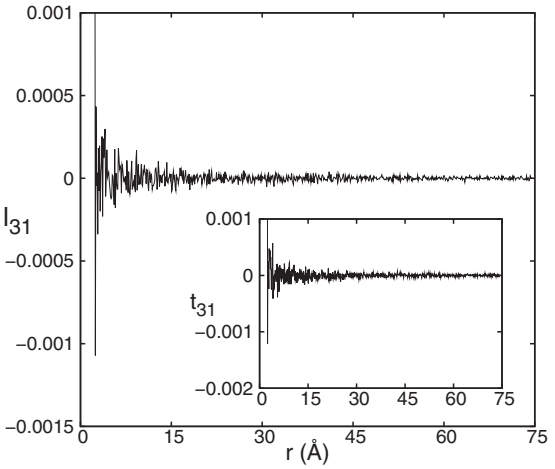

FIG. 6. TIP5P: l_{31}, (*inset*) t_{31}. Longitudinal and transverse parts of correlation $\langle \hat{e}_3 \hat{e}_1 \rangle$, vanishing upto statistical errors after the first solvation peak

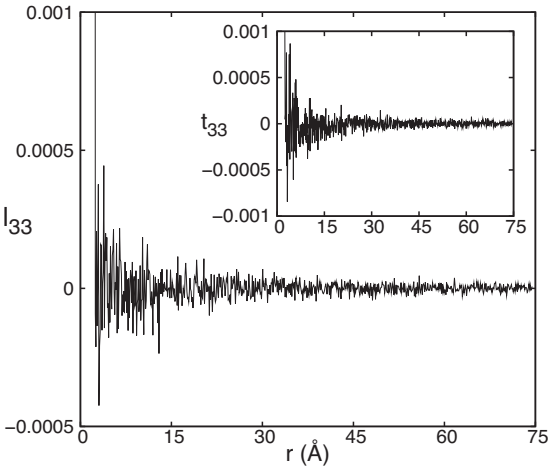

FIG. 8. TIP5P: l_{33}, (*inset*) t_{33}. Longitudinal and transverse parts of correlation $\langle \hat{e}_3 \hat{e}_3 \rangle$, vanishing upto statistical errors after the first solvation peak

The orientations of (dipolar) field $\hat{e}_1$ are analyzed by the correlations $\langle e_1^i(\mathbf{r}_1) e_1^j(\mathbf{r}_2) \rangle$ [Eq. (2)] where i,j refer to components of $\hat{e}_1$ vector. This is conveniently decomposed into two parts: transverse trace part $t_{11}(r) = \langle \hat{e}_1(\mathbf{r}_1) \cdot \hat{e}_1(\mathbf{r}_2) \rangle$ measures the dipoles' alignment with respect to each other and thus solely contributes to Kirkwood dielectric function [12–14]; and longitudinal traceless part $l_{11}(r) = \langle \hat{e}_1(\mathbf{r}_1) \cdot \hat{\mathbf{r}} \hat{e}_1(\mathbf{r}_2) \cdot \hat{\mathbf{r}} \rangle$ is a measure of alignment of the vectors with respect to radial vector separating them.

The transverse correlation function $t_{11}(r)$ shows oscillatory solvation structure, but vanishes (in compliance with the rotational symmetry in the full system) beyond 14 Å (Fig. 9). The function $l_{11}(r)$ is seen to be always positive and furthermore, in the 14–75 Å regime it can be fitted to an Ornstein-Zernike (OZ) form as,

$$l_{11}(r) = 0.39(2) \frac{e^{-r/5.2(1)\ \text{Å}}}{r} + 0.027(1) \frac{e^{-r/24(1)\ \text{Å}}}{r}$$

$$r > 14\ \text{Å} \tag{3}$$

$l_{11}(r)$ shows longest correlation length of 24 Å. Furthermore it exhibits solvation peaks upto 14 Å (Fig. 10). The error bars are quoted as explained in the following illustration. Eg. The precise strength of first exponential 0.397541 ± 0.02168 is written here as 0.39(2) which expresses the mean value and in bracket, the error in the last significant digit. The statistical sampling errors dramatically reduce as we go to large distances (as expected) [see Appendix A].

TIP3P model [15], by design, has $\hat{e}_1$ degree of freedom only, i.e., each water molecule's orientation can be completely described by $\hat{e}_1$ field alone (Fig. 1). The simulations on TIP3P water system are performed using NAMD (version 2.6) [16]. Here, 33105 water molecules are simulated in a cubical box of size 100 Å and the procedures employed for collecting equilibriated configurations are same as those described in case of TIP5P. The constrained model is implemented using SETTLE algorithm. Analysis in this case too shows that $t_{11}(r)$ vanishes beyond solvation region, whereas $l_{11}(r)$ follows the same asymptotic behavior as described by Eq. (3). We also find that in the temperature range 280–350 K the strength of the correlation function monotonically decreases with increasing temperature, while the correlation lengths show no significant variation [see Appendix A].

A water molecule in liquid phase is predominantly influenced by hydrogen bonding (short-range interaction) and further, it has a net dipole moment which interacts through long-range Coloumbic forces. We would like to ascertain whether the long-distance behavior of $l_{11}(r)$ is due to the short-range hydrogen-bond interactions or the long-range Coloumbic interactions [17,18]. To test this possibility, the Coulombic interactions are smoothly truncated at 12 Å in TIP3P model, thus retaining an effective short-range interaction alone. We find that $l_{11}(r)$ remains essentially unchanged in the regions of first few solvation shells and $r > 30$ Å [see

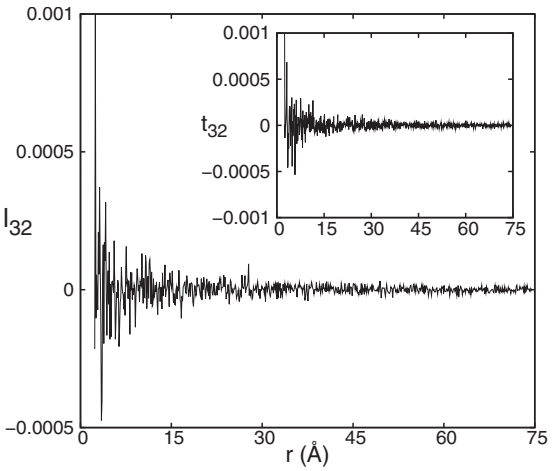

FIG. 7. TIP5P: l_{32}, (*inset*) t_{32}. Longitudinal and transverse parts of correlation $\langle \hat{e}_3 \hat{e}_2 \rangle$, vanishing upto statistical errors after the first solvation peak

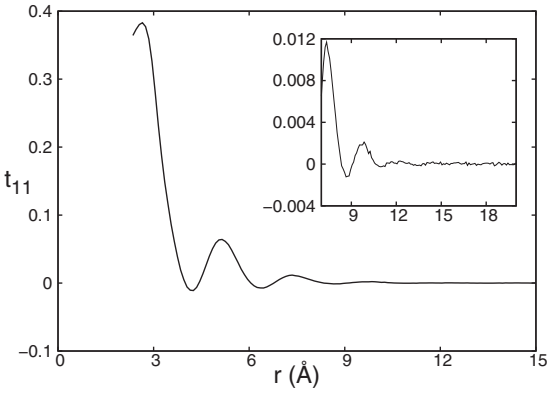

FIG. 9. TIP5P: $t_{11}(r)$. Dipole-dipole transverse trace part showing all the solvation peaks. (*inset*) The correlation vanishes beyond the solvation region of 14 Å

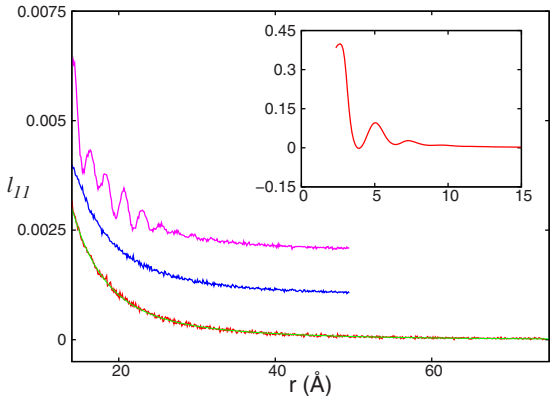

FIG. 10. (Color online) Exponential decay in longitudinal dipole-dipole correlation $l_{11}(r)$ of liquid water outside the solvation region. (*red and green*, right on top of each other; lower) TIP5P data and fit function given by Eq. (3). (*blue; middle*) TIP3P data. (*pink; upper*) TIP3P with truncated Coulombic interactions. For clarity, the middle and upper curves are shifted up by 0.001 and 0.002 units, respectively. (*inset*) $l_{11}(r)$ inside the solvation region within TIP5P model.

Appendix A]. The intermediate region exhibits overstructuring effects upto 30 Å, as seen earlier [19,20].

The above three cases are in agreement with Eq. (3) asymptotically. These observations suggest that (i) water in liquid phase has fluctuations only in dipole degree of freedom; in contrast, the quadrupole has no effect beyond the first solvation peak; (ii) these dipole fluctuations in liquid water are influenced by local environment of respective molecule through hydrogen bonding, significantly more compared to long-range electrostatic interactions; and (iii) furthermore, the dipole fluctuations exhibit long-distance correlations.

Here we briefly mention the status of experimental and other numerical observations of various correlations in liquid water. No direct experimental determination of correlation lengths exist. The much-studied correlation function $g(r)$ for water shows only solvation peaks; although recent small-angle x-ray scattering experiments indicate that $g(r)$ has a correlation length of about 3 Å (300 K) [21] in corroboration with an earlier small-angle neutron-scattering experiment [22]. The origin of this length is speculated to be due to presence of low-dense and high-dense hydrogen-bonded structures coexisting in liquid water [21] (this effect is absent in our simulations). As far as dipole-dipole correlations $t_{11}(r)$ and $l_{11}(r)$ are concerned, to our knowledge, there has been no direct experimental determination of the correlation lengths to the precision required; in particular, the large correlation lengths in $l_{11}(r)$. Indeed the only long-range effect seen in liquid water is that of attraction between two hydrophobic surfaces felt at distances as far as 200 Å [23]. In case of rough hydrophobic surfaces this force is observed even at a distance of about a micrometer [24]. In MD simulations using spherically symmetric models of water [25–30] the interesting correlation is $g(r)$, which exhibits solvation peaks without any significant long-distance behavior; supporting the view that any long-range correlation in water can only be due to dipole degree of freedom.

In the following section we consider the effect of the observed long-range correlations in liquid water on the solvation behavior of mesoscopic hydrophobic surfaces.

Hydrophobic effect: the first notable mechanism postulated to describe the origin of hydrophobic effect came from solvation studies of Frank and Evans in the name of "iceberg" model [31] and later, the same effect has been elucidated by Kauzmann on its possible biological implications [32]. This phenomenon, in its various manifestations, has been extensively discussed in recent literature [5,6,33–35]. The simulation studies on water using various potentials focused on short-range properties of hydrophobic effect and thermodynamics of hydrophobes' solvation [36–39]. The generality of these properties in fluids with characteristic intermolecular attractions was qualitatively explained by theoretical studies [40–44]. In experiments the long-range properties of the hydrophobic force were studied using a combination of surface force apparatus (SFA) and atomic force microscopy (AFM) techniques. In this context an early experiment in 80s revealed a force of attraction between two nominally hydrophobic macroscopic surfaces and found that in the range 10 Å to 100 Å the force falls off exponentially with a correlation length of 12 Å [45]. Later there have been several such studies with surfaces prepared and characterized using wide range of techniques [5,23]. Yet there were very few theoretical developments to explain qualitatively different force profiles observed in experiments. Theories addressing long-range nature of the force relied on phenomena such as cavitation due to metastability of confined fluid [46–48], attraction induced by formation of liquid-vapor-like interface near surfaces [33,49], bridging of nanobubbles [50–52], surface-induced dipolar correlations propagating into bulk [53,54] and so on. Observations from one of the recent experiments [5] with smooth stable hydrophobic surfaces suggest that the attraction at short distances common to all types of surfaces is exponentially decaying within distance regime of 10–100 Å. We address here this monotonic attractive force in the context of mesoscopic surfaces and attribute it to the large lengthscale equilibrium dipolar fluctuations observed in pure liquid water.

Hydrophobic surfaces cannot form hydrogen bonds with the surrounding water, consequently water molecules rear-

range themselves such that they form a sheet of hydrogen-bond network on the surface. Their interactions are such that the directions of lone pairs and hydrogen atoms are perpendicular to the surface normal of the hydrophobe. Owing to the approximate tetrahedral conformation, water molecules cannot have a unique configuration satisfying the above criterion [55]. Consequently they explore other possible orientations as well by fluctuating at the picosecond time scales [56–58]. These network fluctuations contribute significantly to the free energy of solvation of the hydrophobe. In presence of two such hydrophobes, as noted earlier, the range of the force acting between them is large i.e., over a scale >100 Å and to numerically observe this effect a system with about a million atoms needs to be simulated, which is computationally very expensive. Alternatively, a quantitative theoretical estimate is considered below.

Interaction between hydrophobic surface and solvent water can be written in terms of $\hat{n}(\mathbf{r})$, the local unit normal vector to the hardcore van der Waals surface of the hydrophobe and $\hat{e}_1(\mathbf{r}')$, the dipole of water molecule near the surface, where $\mathbf{r}'=\mathbf{r}+\delta\mathbf{r}$; $\delta\mathbf{r}$ is typical length of hydrogen arm of water molecule (about 1 Å). A simple local interaction term can be taken as $(\hat{n}(\mathbf{r})\cdot\hat{e}_1(\mathbf{r}'))^2$ implying that the water dipoles orient orthogonal to the surface normal as seen in simulations [59–61] (importantly, no linear term in $(\hat{n}\cdot\hat{e}_1)$, for that means a preferential orientation of the water dipole inward/outward to the surface).

The change in free energy due to purely hydrophobic interaction between two small surfaces S_1 and S_2 (Fig. 11) in water can be estimated by

$$e^{-\Delta G/kT}=\langle e^{-\Delta H/kT}\rangle$$

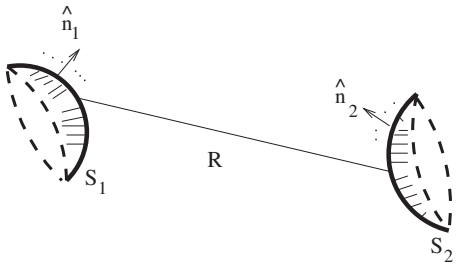

FIG. 11. S_1, S_2 are hydrophobic surfaces with their local normal vectors $\hat{n}_1$, $\hat{n}_2$. "R" is the minimum distance between the two surfaces

$$\Delta H=\frac{\gamma_1}{2}\int_{S_1} d\hat{n}_1(\hat{n}_1(\mathbf{r}_1)\cdot\hat{e}_1(\mathbf{r}_1'))^2+\frac{\gamma_2}{2}\int_{S_2} d\hat{n}_2(\hat{n}_2(\mathbf{r}_2)\cdot\hat{e}_1(\mathbf{r}_2'))^2 \tag{4}$$

γ is a measure of strength of interaction between hydrophobic solute and water which can depend upon temperature, density and other parameters defining the thermodynamic system. The brackets $\langle\ldots\rangle$ refer to statistical averaging with respect to pure water system and integration is over area of each surface. As illustrated in Fig. 11, S_1, S_2 refer to two arbitrary hydrophobic surfaces and $\mathbf{R}$ is a vector along minimum distance of separation between them.

When the distance $R(=|\mathbf{R}|)$ is large compared to radius of curvature of each surface and the surface areas sufficiently small, the statistical averaging can be done by cumulant expansion. The leading term of the force $F(R)=-\partial\Delta G/\partial R$ is given by the following equation [see Appendix B],

$$F(R)\simeq\frac{\gamma_1\gamma_2}{2kT}\frac{\partial}{\partial R}\int_{S_1}\int_{S_2} d\hat{n}_1 d\hat{n}_2\langle[\hat{n}_1(\mathbf{r}_1)\cdot\hat{e}_1(\mathbf{r}_1')\hat{n}_2(\mathbf{r}_2)\cdot\hat{e}_1(\mathbf{r}_2')]^2\rangle=\frac{\gamma_1\gamma_2}{2kT}A_1A_2\frac{\partial}{\partial R}Tr[\mathbf{\Sigma_{S_1}E}(\mathrm{R})\mathbf{\Sigma_{S_2}E}(\mathrm{R})] \tag{5}$$

where A_1, A_2 are areas of the surfaces and the matrices $\mathbf{E}$, $\mathbf{\Sigma_S}$ are given by

$$E^{ij}(R)\equiv\langle e_1^i(\mathbf{r}_1')e_1^j(\mathbf{r}_2')\rangle\simeq-\frac{1}{2}\left(\delta^{ij}-3\frac{R^iR^j}{R^2}\right)l_{11}(R)\quad\text{for large } R$$

$$\Sigma_S^{ij}\equiv\frac{1}{A}\int_S d\hat{n}n^in^j$$

$\mathbf{\Sigma_S}$ is a geometric factor characteristic of shape of the surface [see Appendix C].

The above result on hydrophobic force is very general in nature. As discussed in earlier paragraphs, the leading order $(\hat{n}\cdot\hat{e}_1)^2$ is taken to be the interaction energy term for simplicity. By including the nonleading terms in the interaction energy function [Eq. (4)] and doing the cumulant expansion, it can be shown that the force term [Eq. (5)] for large R remains unchanged, thus establishing the generality of the result.

These considerations are valid for distances beyond the solvation region of a typical water molecule. The cumulant expansion allowed decomposing the force equation as a simple convolution of surface-dependent part and water-dependent part. Equation (5) enables us to conclude that range of the force between hydrophobic surfaces at large distances is always attractive governed by $l_{11}^2(R)\propto e^{-R/12}$ for large R. Therefore the hydrophobic force falls off exponentially with a largest correlation length of about 12 Å [see

TABLE I. Numerical fitting of $l_{11}(r)$ obtained from simulations of TIP5P and TIP3P data. The error bars quoted are as per the following illustration: e.g., $0.397\,541 \pm 0.021\,68$ is written as 0.39(2) which expresses the mean value and its leading significant deviation.

Model	Fit function $f(r)$	RMSD
TIP5P	$0.39(2)\frac{e^{-r/5.2(1)}}{r} + 0.027(1)\frac{e^{-r/24(1)}}{r}$	2.54462e−05
TIP3P	$0.34(2)\frac{e^{-r/5.4(2)}}{r} + 0.029(3)\frac{e^{-r/24(1)}}{r}$	2.54122e−05
TIP5P	$0.152(2)\frac{e^{-r/10.36(9)}}{r}$	5.33897e−05
TIP3P	$0.151(2)\frac{e^{-r/10.5(1)}}{r}$	5.80041e−05
TIP5P	$0.0220(4)e^{-r/6.71(5)}$	6.72991e−05
TIP3P	$0.0217(5)e^{-r/6.85(6)}$	7.78593e−05
TIP5P	$\frac{8.0(1)}{r^{2.990(8)}}$	2.5292e−05
TIP3P	$\frac{7.2(1)}{r^{2.940(8)}}$	2.5860e−05

Appendix B], in addition to several other shorter range exponents as well,

$$F(R) \propto -e^{-R/12\ \text{Å}} \quad \text{for large } R, \tag{6}$$

The strength of attraction is proportional to area A and shape of each surface given by the tensor $\mathbf{\Sigma}$, the second moment of surface normal. The final trace operation over the matrices $\mathbf{E}(\mathrm{R})$ and $\mathbf{\Sigma}_\mathbf{S}$ [as in Eq. (5)] implies that the hydrophobic attraction is not just a purely distance-dependent interaction such as van der Waals'. Indeed the orientation of the surface shapes relative to each other can modify this force significantly. As an example if two small planar hydrophobic surfaces are mutually perpendicular and are sufficiently far apart, there should be no force between them as opposed to when they face each other [see Appendix C].

Our systematic analysis of data from MD simulation of liquid water clearly shows that only longitudinal dipole-dipole correlation exhibits long-range behavior with correlation lengths of about 5 and 24 Å [Eq. (3)]. Experimental validation of this correlation has eluded many efforts mainly because in a generic light-scattering experiment photons couple to dipole of water molecules and the leading scattering effect comes from the transverse correlation only. Therefore we considered indirect effects of the longitudinal dipolar fluctuations; of which the promising candidate seems to be the "hydrophobic force." It is well known that the nature of hydrophobic force between macroscopic surfaces is very different from that of mesoscopic surfaces [33]. These differences need to be analyzed either with MD simulation or modeling hydrogen-bond network interactions in liquid water. A simple-minded theoretical estimate of the force between mesoscopic hydrophobic surfaces done here suggests that the surfaces do experience a long-range force albeit the strength is not large and in addition, the proposed force depends on shape and relative orientations of the surfaces. It would be an interesting challenge to device AFM type of setup to validate this phenomenon experimentally.

Computer time on Vindhya and KABRU computing clusters at the Institute of Mathematical Sciences is greatly appreciated.

APPENDIX A

Theoretical considerations suggest that in any statistical system at thermal equilibrium, fluctuating modes in three-dimensional space will generate correlations of Ornstein-Zernike (OZ) form, i.e., $\frac{e^{-r/\xi}}{r}$; for example, Debye correlation in a plasma of ions. There may indeed be more than one such mode in a system. If they are weakly interacting modes, their strength coefficients would all be positive as in Eq. (3). For completeness other fit functions are also tried on $l_{11}(r)$ data. Their corresponding root-mean-square deviations (RMSDs) and the tested models are summarized in Table I.

Among the exponentials, the biexponential OZ function has at least a factor of two better RMSD than other combinations. A single power law also seems to fit the data very well in this limited distance range upto 75 Å. However, if this behavior is extrapolated asymptotically for large distances, it amounts to the fact that the system is exhibiting critical behavior. But in MD simulations, we did not see any concomitant signatures of critical behavior at all. Furthermore, liquid water is certainly not critical at ambient conditions. Therefore, we discard the power-law extrapolation and conclude that the biexponential OZ fit function is the correct extrapolation.

The above comparison between various fitting functions, to ascertain the asymptotic behavior of the $l_{11}(r)$ correlation, does not cleanly discard one fit function over the other. From numerics point of view $1/r^3$ fit cannot be strictly ruled out. In dipolar fluids linear-response theories propose the exis-

TABLE II. TIP3P: $l_{11}(r)$ temperature dependence and corresponding variation in fit function parameters.

T ($P=1$ atm) (K)	Fit function	RMSD
280	$0.42(3)\frac{e^{-r/5.0(2)}}{r}+0.031(3)\frac{e^{-r/24(1)}}{r}$	3.3018e−05
	$\frac{6.9(1)}{r^{2.90(1)}}$	3.4272e−05
	$\frac{9.00(1)}{r^3}$	3.8138e−05
300	$0.34(2)\frac{e^{-r/5.4(2)}}{r}+0.029(3)\frac{e^{-r/24(1)}}{r}$	2.5412e−05
	$\frac{7.2(1)}{r^{2.940(8)}}$	2.5870e−05
	$\frac{8.58(1)}{r^3}$	2.7774e−05
350	$0.31(2)\frac{e^{-r/5.6(3)}}{r}+0.023(3)\frac{e^{-r/27(3)}}{r}$	3.3624e−05
	$\frac{6.3(2)}{r^{2.92(1)}}$	3.4253e−05
	$\frac{7.93(1)}{r^3}$	3.6437e−05

tence of such a power-law behavior attributed to the presence of Coulombic interactions [17].

This motivated us to investigate the origin of the long-range behavior. In the simulation it is possible to make the Coulombic interactions vanish smoothly beyond a certain distance. We did so here at a distance of 12 Å; thereby retaining an effective short-range interaction alone which still reproduces the known solvation peaks in $g(r)$ accurately. Consequently we can envisage the situation where short-range solvation peaks are kept untouched and the long-range Coulombic forces made to vanish. Then the linear-response theory would suggest that the long-range behavior in $l_{11}(r)$ should alter. However we notice that the Coulombic truncation has null effect quantitatively on the long-range nature of $l_{11}(r)$. Hence we conclude that the $1/r^3$ behavior is not the correct way to extrapolate to large distances.

Also, we studied the effect of temperature on various extrapolations within TIP3P model [Table II]. This analysis showed that the long-range behavior of $l_{11}(r)$ responds to the variation in temperature (and hence density) of the system; in contradiction with the linear-response theories which predict a net change in strength only, not in the $1/r^3$ nature of correlation.

APPENDIX B

We give briefly the intermediate steps to deduce the force equation in this section. The technique under consideration is cumulant expansion used to perform statistical averaging in an approximate manner [62]. Formally the exponential term may be expanded as follows:

$$\frac{Z_S}{Z}=\left\langle\left[1-\frac{1}{kT}\frac{\gamma_1}{2}\int_{S_1}d\hat{n}_1(\hat{n}_1(\mathbf{r}_1)\,.\,\hat{e}_1(\mathbf{r}_1'))^2+\gamma_1^2\cdots\right]\left[1-\frac{1}{kT}\frac{\gamma_2}{2}\int_{S_2}d\hat{n}_2(\hat{n}_2(\mathbf{r}_2)\,.\,\hat{e}_1(\mathbf{r}_2'))^2+\gamma_2^2\cdots\right]\right\rangle$$
$$=\left\langle 1-\gamma_1(\ldots)-\gamma_2(\ldots)+\frac{\gamma_1\gamma_2}{4(kT)^2}\int_{S_1}\int_{S_2}d\hat{n}_1d\hat{n}_2(\hat{n}_1(\mathbf{r}_1)\,.\,\hat{e}_1(\mathbf{r}_1'))^2(\hat{n}_2(\mathbf{r}_2)\,.\,\hat{e}_1(\mathbf{r}_2'))^2+\cdots\right\rangle.$$

In the above expression, the constant term signifies no change in free energy w.r.t. pure system. The linear term in γs' give contribution to the surface energy, which we will not consider here as they do not contribute to the force. The bilinear term, proportional to $\gamma_1\gamma_2$, is the distance-dependent contribution to free energy due to interaction between surfaces. The force between the surfaces arises solely from terms of this kind.

Now, the last expression can be written as exponential over averages, as follows:

$$e^{-\Delta G/kT} \equiv \frac{Z_S}{Z} = \exp\left[\gamma_1\langle\cdots\rangle + \gamma_2\langle\cdots\rangle + \frac{\gamma_1\gamma_2}{4(kT)^2}\int_{S_1}\int_{S_2} d\hat{n}_1 d\hat{n}_2 \langle(\hat{n}_1(\mathbf{r}_1)\,.\,\hat{e}_1(\mathbf{r}_1'))^2(\hat{n}_2(\mathbf{r}_2)\,.\,\hat{e}_1(\mathbf{r}_2'))^2\rangle + \cdots \right]$$

force between the surfaces is given by

$$F(R) = -\frac{\partial \Delta G}{\partial R} \simeq \frac{\gamma_1\gamma_2}{4kT}\frac{\partial}{\partial R}\int_{S_1}\int_{S_2} d\hat{n}_1 d\hat{n}_2 \langle(\hat{n}_1(\mathbf{r}_1)\,.\,\hat{e}_1(\mathbf{r}_1'))^2(\hat{n}_2(\mathbf{r}_2)\,.\,\hat{e}_1(\mathbf{r}_2'))^2\rangle$$

where we have explicitly retained the leading contribution for large R.

Employing the notation that any repeated index is summed over,

$$(\hat{n}_1\,.\,\hat{e}_1)^2 \equiv n_1^i e_1^i n_1^j e_1^j$$

$$(\hat{n}_2\,.\,\hat{e}_1)^2 \equiv n_2^k e_1^k n_2^l e_1^l$$

$$\begin{aligned}
&\frac{\partial}{\partial R}\langle(\hat{n}_1(\mathbf{r}_1)\,.\,\hat{e}_1(\mathbf{r}_1')^2(\hat{n}_2(\mathbf{r}_2)\,.\,\hat{e}_1(\mathbf{r}_2'))^2\rangle \\
&= \frac{\partial}{\partial R}\langle n_1^i e_1^i(\mathbf{r}_1') n_1^j e_1^j(\mathbf{r}_1') n_2^k e_1^k(\mathbf{r}_2') n_2^l e_1^l(\mathbf{r}_2')\rangle \\
&= n_1^i n_1^j n_2^k n_2^l \frac{\partial}{\partial R}\langle e_1^i(\mathbf{r}_1') e_1^j(\mathbf{r}_1') e_1^k(\mathbf{r}_2') e_1^l(\mathbf{r}_2')\rangle \\
&= n_1^i n_1^j n_2^k n_2^l \frac{\partial}{\partial R}[2\langle e_1^i(\mathbf{r}_1') e_1^k(\mathbf{r}_2')\rangle\langle e_1^l(\mathbf{r}_2') e_1^j(\mathbf{r}_1')\rangle \\
&\quad + \{\langle e_1^i(\mathbf{r}_1') e_1^j(\mathbf{r}_1') e_1^k(\mathbf{r}_2') e_1^l(\mathbf{r}_2')\rangle - 2\langle e_1^i(\mathbf{r}_1') e_1^k(\mathbf{r}_2')\rangle \\
&\quad \times\langle e_1^l(\mathbf{r}_2') e_1^j(\mathbf{r}_1')\rangle\}]
\end{aligned}$$

where i,j,k,l are vector indices.

The last step is tautological as we added and subtracted an important term in the expression. Furthermore, it can be shown that in a system where asymptotic behavior of correlation $\langle e_1^i(\mathbf{r}_1') e_1^k(\mathbf{r}_2')\rangle$ is exponentially falling off, the last term $\{\ldots\}$ in the last expression falls off exponentially even faster than the first term and therefore it can be neglected in the asymptotic region (i.e., for large R).

The vector indices imply matrix multiplication and a *trace* operation over the product of matrices coming from j index summation. This should be clear if we define the matrices,

$$E^{ij}(R) = \langle e_1^i(\mathbf{r}_1') e_1^j(\mathbf{r}_2')\rangle$$

$$(\Sigma_S)^{ij} = \frac{1}{A}\int_S d\hat{n}\, n^i n^j$$

where i,j are generic vector indices and R is the minimum distance of separation. Now the force expression takes the form,

$$F(R) = \frac{\gamma_1\gamma_2}{2kT} A_1 A_2 \frac{\partial}{\partial R}\mathrm{Tr}[\boldsymbol{\Sigma}_{\mathbf{S_1}}\mathbf{E}(\mathrm{R})\boldsymbol{\Sigma}_{\mathbf{S_2}}\mathbf{E}(\mathrm{R})] \qquad \text{(B1)}$$

where Tr[...] means *trace* over the product of matrices. The subscripts S_1 and S_2 refer to respective surfaces and Σ matrix defines the second moment of surface normal over the respective surface.

Now, from Eq. (2),

$$E^{ij}(r) = \frac{1}{2}\left(\delta^{ij} - \frac{r^i r^j}{r^2}\right) t_{11}(r) - \frac{1}{2}\left(\delta^{ij} - 3\frac{r^i r^j}{r^2}\right) l_{11}(r)$$

Our analysis from simulation of bulk liquid water shows that at large distances (R), only longitudinal part of dipolar correlations survives, i.e.,

$$E^{ij}(R) \simeq -\frac{1}{2}\left(\delta^{ij} - 3\frac{R^i R^j}{R^2}\right) l_{11}(R) \quad \text{where}$$

$$l_{11}(R) = 0.39\frac{e^{-R/5.2}}{R} + 0.027\frac{e^{-R/24}}{R} \quad R > 14 \text{ Å}.$$

Hence, the force equation [Eq. (5)] will take the form

$$\begin{aligned}
F(R) &\sim \mathrm{const}\frac{\partial}{\partial R}\mathrm{Tr}[\ldots] l_{11}^2(R) \\
&\sim (-)\mathrm{const} \times \mathrm{Tr}[\ldots]\frac{1}{R^2}\exp(-R/12 \text{ Å})
\end{aligned}$$

where, only the long-range exponential's contribution is emphasized, as analysis is for large distances of separation i.e., large R only.

APPENDIX C

The $\boldsymbol{\Sigma}$ matrix is a geometric factor related to second moment of the surface normal. It is defined as

$$(\Sigma_S)^{ij} \equiv \frac{1}{A}\int_S d\hat{n} n^i n^j$$

where $\hat{n}(\mathbf{r})$ is the local normal vector at the point $\mathbf{r}$ on the surface; i,j are any two out of three vector components of $\hat{n}$.

For a segment of spherical surface, as illustrated by Fig. 12,

$$\hat{n}{:}(\sin\theta\cos\phi, \sin\theta\sin\phi, \cos\theta);$$

$$A_S = \int_S d\hat{n} = \int_0^{\bar{\theta}} d\theta \sin\theta \int_0^{2\pi} d\phi = 2\pi(1-\cos\bar{\theta})$$

The integral $\int n^i n^j$ can be carried out in a similar manner over various pairs of $\hat{n}$ vector components. The $\boldsymbol{\Sigma}$ matrix can be

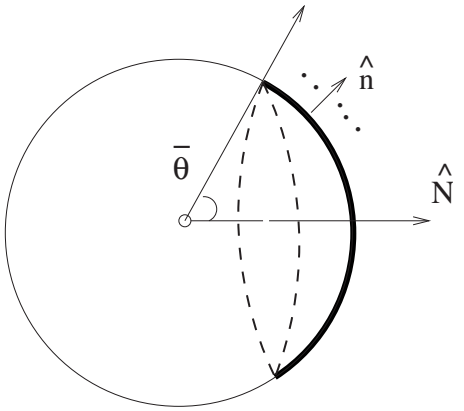

FIG. 12. A segment of spherical surface (boldened). $\hat{n}$ is local normal vector, and $\bar{\theta}$ is the sector angle for the segment. $\hat{N}$ is the dipole vector of the segment, obtained by integrating $\hat{n}$ over the extent of segment surface [see Appendix C].

finally expressed in terms of first moment of the surface as follows:

$$(\Sigma_S)^{ij} = \frac{1}{A}\int_S d\hat{n} n^i n^j = \frac{1}{3}\delta^{ij} - \frac{1}{6}\cos\bar{\theta}(1+\cos\bar{\theta})(\delta^{ij} - 3N^i N^j)$$

$$N^i = \frac{M^i}{|M|}, \quad M^i = \frac{1}{A}\int_S d\hat{n} n^i$$

For a sphere, $\bar{\theta}=\pi$. Hence $\Sigma^{ij}=\frac{1}{3}\delta^{ij}$.

For a plane, $\bar{\theta}=0$. Hence $\Sigma^{ij}=N^i N^j$.

The direction of $\hat{N}$ is chosen only w.r.t. the side of surface under consideration.

We show below that the strength of the force depends on the relative orientations of the surfaces w.r.t. each other. We consider two planar surfaces separated by large distance inside aqueous medium. For the surface S_1, $\Sigma_1^{ij}=N_1^i N_1^j$ and similarly for S_2, $\Sigma_2^{kl}=N_2^k N_2^l$ where i,j,k,l are dummy indices over three dimensions in coordinate space. For large R, $E^{ij}(R) \simeq -\frac{1}{2}(\delta^{ij} - 3\frac{R^i R^j}{R^2}) l_{11}(R)$ where i,j are dummy vector indices.

So, the part of force expression involving convolution of $\mathbf{\Sigma}_S$ and $\mathbf{E}$ matrices reads as,

$$F_{\text{large } R} \propto (-)\mathrm{Tr}\left[N_1^i N_1^j \left(\delta^{jk} - 3\frac{R^j R^k}{R^2} \right) \times N_2^k N_2^l \left(\delta^{li} - 3\frac{R^l R^i}{R^2} \right) \right] \frac{e^{-R/12}}{R^2}$$

$$\propto (-)[\hat{N}_1 \cdot \hat{N}_2 - 3(\hat{N}_1 \cdot \hat{\mathbf{R}})(\hat{N}_2 \cdot \hat{\mathbf{R}})]^2 \frac{e^{-R/12}}{R^2}$$

For surfaces parallel to each other, $\hat{N}_1 \cdot \hat{N}_2 = \hat{N}_1 \cdot \hat{\mathbf{R}} = \hat{N}_2 \cdot \hat{\mathbf{R}} = 1$. Hence $F \propto (-)\frac{e^{-R/12}}{R^2}$.

For surfaces perpendicular to each other, $\hat{N}_1 \cdot \hat{N}_2 = 0$ and either $\hat{N}_1 \cdot \hat{\mathbf{R}} = 0$ or $\hat{N}_2 \cdot \hat{\mathbf{R}} = 0$ depending on orientation of respective surface w.r.t. the radial unit vector. Hence $F=0$.

[1] C. J. Fecko *et al.*, Science **301**, 1698 (2003).
[2] F. W. Starr, J. K. Nielsen, and H. E. Stanley, Phys. Rev. Lett. **82**, 2294 (1999).
[3] F. N. Keutsch and R. J. Saykally, Proc. Natl. Acad. Sci. U.S.A. **98**, 10533 (2001).
[4] F. H. Stillinger, Science **209**, 451 (1980).
[5] E. E. Meyer, K. J. Rosenberg, and J. N. Israelachvili, Proc. Natl. Acad. Sci. U.S.A. **103**, 15739 (2006).
[6] P. Ball, Chem. Rev. (Washington, D.C.) **108**, 74 (2008).
[7] M. W. Mahoney and W. L. Jorgensen, J. Chem. Phys. **112**, 8910 (2000).
[8] S. Rick, J. Chem. Phys. **120**, 6085 (2004).
[9] E. Lindahl, B. Hess, and D. van der Spoel, J. Mol. Model. **7**, 306 (2001).
[10] D. Frenkel and B. Smit, *Understanding Molecular Simulation*, Computational Science Series (Academic Press, New York, 2001), Vol. 1.
[11] A. Leach, *Molecular Modelling: Principles and Applications*, 2nd ed. (Prentice Hall, New York, 2001).
[12] J. G. Kirkwood, J. Chem. Phys. **7**, 911 (1939).
[13] M. Sharma, R. Resta, and R. Car, Phys. Rev. Lett. **98**, 247401 (2007).
[14] P. L. Silvestrelli and M. Parrinello, Phys. Rev. Lett. **82**, 3308 (1999).
[15] W. L. Jorgensen *et al.*, J. Chem. Phys. **79**, 926 (1983).
[16] L. Kale *et al.*, J. Comput. Phys. **151**, 283 (1999).
[17] J.-P. Hansen and I. R. McDonald, *Theory of Simple Liquids*, 3rd ed. (Academic Press, U.K., 2006).
[18] G. Mathias and P. Tavan, J. Chem. Phys. **120**, 4393 (2004).
[19] M. P. Allen and D. J. Tildesley, *Computer Simulation of Liquids*, 1st ed., Oxford Science Publications (Clarendon Press, Oxford, 1987).
[20] J. Kolafa and I. Nezbeda, Mol. Phys. **98**, 1505 (2000).
[21] C. Huang *et al.*, Proc. Natl. Acad. Sci. U.S.A. **106**, 15214 (2009).
[22] L. Bosio, J. Teixeira, and H. E. Stanley, Phys. Rev. Lett. **46**, 597 (1981).
[23] H. K. Christenson and P. M. Claesson, Adv. Colloid Interface Sci. **91**, 391 (2001).
[24] S. Singh, J. Houston, F. van Swol, and C. J. Brinker, Nature (London) **442**, 526 (2006).
[25] A. B. de Oliveira, P. A. Netz, T. Colla, and M. C. Barbosa, J. Chem. Phys. **125**, 124503 (2006).
[26] T. Head-Gordon and F. H. Stillinger, J. Chem. Phys. **98**, 3313 (1993).
[27] E. A. Jagla, J. Chem. Phys. **111**, 8980 (1999).
[28] W. P. Krekelberg, T. Kumar, J. Mittal, J. R. Errington, and T. M. Truskett, Phys. Rev. E **79**, 031203 (2009).
[29] R. M. Lynden-Bell and P. G. Debenedetti, J. Phys. Chem. B **109**, 6527 (2005).

[30] Z. Yan, S. V. Buldyrev, N. Giovambattista, and H. E. Stanley, Phys. Rev. Lett. **95**, 130604 (2005).
[31] H. S. Frank and M. W. Evans, J. Chem. Phys. **13**, 507 (1945).
[32] W. Kauzmann, Adv. Protein Chem. **14**, 1 (1959).
[33] D. Chandler, Nature (London) **437**, 640 (2005).
[34] M. Chaplin, Nat. Rev. Mol. Cell Biol. **7**, 861 (2006).
[35] K. A. Dill, T. M. Truskett, V. Vlachy, and B. Hribar-Lee, Annu. Rev. Biophys. Biomol. Struct. **34**, 173 (2005).
[36] H. S. Ashbaugh, T. M. Truskett, and P. G. Debenedetti, J. Chem. Phys. **16**, 2907 (2002).
[37] S. V. Buldyrev *et al.*, Proc. Natl. Acad. Sci. U.S.A. **104**, 20177 (2007).
[38] F. Despa and R. Berry, Biophys. J. **95**, 4241 (2008).
[39] A. Wallqvist and B. J. Berne, J. Phys. Chem. B **99**, 2885 (1995).
[40] H. S. Ashbaugh and L. R. Pratt, Rev. Mod. Phys. **78**, 159 (2006).
[41] L. R. Pratt and D. Chandler, J. Chem. Phys. **67**, 3683 (1977).
[42] L. R. Pratt and D. Chandler, J. Chem. Phys. **73**, 3434 (1980).
[43] B. Widom and D. Ben-Amotz, Proc. Natl. Acad. Sci. U.S.A. **103**, 18887 (2006).
[44] B. Widom, P. Bhimalapuram, and K. Koga, Phys. Chem. Chem. Phys. **5**, 3085 (2003).
[45] J. N. Israelachvili and R. Pashley, Nature (London) **300**, 341 (1982).
[46] N. F. Bunkin *et al.*, Langmuir **13**, 3024 (1997).
[47] H. K. Christenson and P. M. Claesson, Science **239**, 390 (1988).
[48] V. S. J. Craig, B. W. Ninham, and R. M. Pashley, Langmuir **15**, 1562 (1999).
[49] K. Lum, D. Chandler, and J. D. Weeks, J. Phys. Chem. B **103**, 4570 (1999).
[50] P. Attard, Langmuir **12**, 1693 (1996).
[51] P. Attard, M. P. Moody, and J. W. G. Tyrrell, Physica A **314**, 696 (2002).
[52] J. W. G. Tyrrell and P. Attard, Phys. Rev. Lett. **87**, 176104 (2001).
[53] F. Despa and R. S. Berry, Biophys. J. **92**, 373 (2007).
[54] F. Despa, A. Fernandez, and R. S. Berry, Phys. Rev. Lett. **93**, 228104 (2004).
[55] Y. K. Cheng and P. J. Rossky, Nature (London) **392**, 696 (1998).
[56] P. N. Perera *et al.*, Proc. Natl. Acad. Sci. U.S.A. **106**, 12230 (2009).
[57] A. Poynor, L. Hong, I. K. Robinson, S. Granick, Z. Zhang, and P. A. Fenter, Phys. Rev. Lett. **97**, 266101 (2006).
[58] Y. L. A. Rezus and H. J. Bakker, Phys. Rev. Lett. **99**, 148301 (2007).
[59] P. L. Chau, Mol. Phys. **99**, 1289 (2001).
[60] P. Jedlovszky, J. Phys.: Condens. Matter **16**, S5389 (2004).
[61] T. M. Raschke and M. Levitt, Proc. Natl. Acad. Sci. U.S.A. **102**, 6777 (2005).
[62] N. Goldenfeld, *Lectures on Phase Transitions and the Renormalization Group*, Frontiers in Physics (Perseus Books, U.S.A., 1992).